

Research article

Effect of graphene oxide and ionic liquid on the sliding wear and abrasion resistance of injection molded PMMA nanocomposites

Luis-Francisco Minguez-Enkovaara, Francisco-Jose Carrión-Vilches, María-Dolores Avilés, María-Dolores Bermúdez*

Grupo de Ciencia de Materiales e Ingeniería Metalúrgica Universidad Politécnica de Cartagena. Campus de la Muralla del Mar, 30202 Cartagena, Spain

Received 12 May 2022; accepted in revised form 26 September 2022

Abstract. New polymethylmethacrylate (PMMA) nanocomposites containing 0.5 wt% graphene oxide (GO), or 1.5 wt% graphene oxide modified with the ionic liquid (IL) 1-octyl-3-methylimidazolium tetrafluoroborate (GOIL) have been processed by extrusion and injection molding to obtain PMMA+GO and PMMA+GOIL, respectively. Raman microscopy and mapping show that the additives align parallel to the flow close to the exterior surfaces, with an almost perpendicular orientation in the central core region. Reciprocating sliding tests have been carried out on the exterior surfaces and also on the surface of core sections of the injected parts. GO prevents surface damage, showing negligible wear on both section surfaces under sliding parallel and perpendicular to the injection flow. In contrast, the performance of PMMA+GOIL depends on the sliding direction. Under multiple scratching, both GO and GOIL reduced residual depth values and increased the viscoelastic recovery of PMMA, thus reducing permanent surface damage. PMMA+GOIL shows the highest viscoelastic recovery and the lowest complex viscosity values. Wear mechanisms are discussed as a function of materials properties, nanofiller type, and orientation and sliding direction.

Keywords: nanocomposites, nanomaterials, graphene oxide, ionic liquid, material testing

1. Introduction

One of the technological purposes in the research and development of new polymer nanocomposites is the reduction of energy loss and material damage due to friction and wear in sliding applications and of surface damage produced by abrasion [1, 2]. Carbon nanophases are studied as reinforcements of different polymer matrices aimed at reducing friction coefficients and material loss. Sun and Du [3] have recently reviewed the state of the tribological studies of graphene nanocomposites.

Polymethylmethacrylate (PMMA) parts are manufactured for applications in many structural, industrial, transport, and even biomedical applications for

which tribological performance is critical. PMMA composites [4] are easily manufactured by melt processing techniques, such as extrusion and injection molding, but their wear and scratch resistance need to be improved [5]. Carbon nanophase fillers such as nanotubes, graphene, and graphene oxide have been added to a PMMA matrix [6–12]. The resistance to damage of the surfaces of the final parts is influenced by nanophase distribution and orientation with respect to the melt flow. A very recent review [13] on fiber-reinforced polymer composites containing graphene reported that they exhibit higher wear resistance than the corresponding materials without graphene.

*Corresponding author, e-mail: mdolores.bermudez@upct.es
© BME-PT

Song *et al.* [14] described the preparation of PMMA nanocomposites by in-situ polymerization, containing up to 1 wt% of graphene oxide (GO) with respect to the monomer. A reduction of the running-in friction coefficient was described for GO content higher than 0.8 wt% to reach the same steady-state friction coefficient as pure PMMA after a short sliding distance. They proposed that the good compatibility between the functional groups of GO and PMMA enhances interfacial strength and improves the tribological performance.

Ionic liquids (ILs), salts that are in liquid state at room temperature, have found many applications in tribology and materials science, including polymer technology [15]. ILs possess a unique combination of outstanding properties, such as their high thermal stability in the fluid state; their ability to act as solvents and surfactants; their plasticizing effect towards thermoplastic polymers; and their curing effect in the case of thermosets.

The plasticizing effect of imidazolium ILs for PMMA, when added in very high proportions (50 vol% ILs), was described by Scott and coworkers [16, 17]. Zhao *et al.*, [18] described the multiple roles of 1-butyl-3-methylimidazolium hexafluorophosphate, which not only acts as a plasticizer and processing aid additive, but also improves the dispersion of multiwalled carbon nanotubes in a PMMA matrix. Recently, 2 wt% ILs have been added to PMMA [19], to improve its resistance to deformation, but no tribological studies were conducted.

Graphene-ionic liquid nanohybrid lubricants have received much attention in recent times [20–22]. The synergistic effect between carbon nanophases and ionic liquids [23, 24] has been demonstrated in lubrication [22], both as neat lubricants and as lubricant additives, and also in the reduction of friction and wear of polymers [3, 25]. IL functionalized GO reduced the friction and wear of epoxy resin [25]. Thin lubricant films formed by graphene dispersed in octylmethylimidazolium ILs have been reported recently [26].

The ionic liquid selected in the present study has previously shown its ability to modify carbon nanophases, in particular carbon nanotubes, to develop new thermoplastic nanocomposites [27, 28] with improved abrasive wear resistance.

The most commonly used processing conditions for these nanocomposites require the use of solvents in order to disperse the additives. However, for practical

applications with a reduced environmental impact, melt processing is an adequate route. A recently published precedent of the present work is the preparation, characterization, and optimization of extrusion parameters for extruded PMMA nanocomposites with graphene oxide and graphene oxide modified by ionic liquid [29].

In the present work, PMMA nanocomposites containing graphene oxide (GO) or graphene oxide previously modified by ionic liquid (GOIL) have been melt-processed by extrusion followed by injection molding, avoiding the use of organic solvents. The main objectives are to study the wear resistance of the new materials under different sliding conditions and to relate the results with variables such as injection flow, nanophase type, and distribution. The main novelty with respect to previous works is the study of the different tribological behavior of different regions of nanocomposite injected parts.

2. Experimental

Injection molding grade polymethylmethacrylate (PMMA) (8N; Evonik AG, Germany) was selected for the present study. Graphene oxide (GO) (lateral size (LD50): 40 μm ; average thickness: 1–2 nm; oxygen content (determined by X-ray photoelectron spectroscopy, XPS): 30% Brunnauer-Emmett-Teller (BET) specific surface area: approx. 400 m^2/g ; average number of layers 1–2) was purchased from Avanzare S.L., Spain. The ionic liquid (IL) used in the present study was 1-octyl-3-methylimidazolium tetrafluoroborate (Iolitec GmbH, Germany) (>99% purity). Graphene oxide modified by ionic liquid (GOIL) was obtained following a general procedure similar to that previously described [29]. The first step was the mechanical mixing of GO and IL (in a 1:2 weight proportion) in an agate mortar. After 10 minutes, the mixture was sonicated for 1 hour, and the solid residue was then washed repeatedly with acetonitrile and dried in a vacuum oven for 32 hours at 70 $^{\circ}\text{C}$.

PMMA pellets were milled using an ultracentrifuge mill (ZM200; Retsch, Germany) and dried in a vacuum oven. A TwinLab 10 mm co-rotating twin-screw micro-extruder (TwinTech Extrusion Ltd, U.K.) was used for the first processing step of PMMA and the new nanocomposites, under a temperature profile between 205 and 245 $^{\circ}\text{C}$ and a specific mechanical energy of 1800 kJ/kg. Extrusion processing parameters were selected according to previous optimization

works [29]. The extruded materials were then cooled to 70 °C and pelletized before injection molding in a DEU (Spain) 250 H55 mini VP machine at 245 °C, under an injection pressure of 120 MPa, with a mold temperature of 65 °C and an injection speed of 10 cm³/s. The injection molding parameters are those recommended for PMMA.

In order to observe the presence of the nanofillers inside the injected parts, images of 1 mm thick sections were taken with a digital camera and edited using GIMP image editing software.

Materials were characterized using a Leica DMRX optical microscope, a Hitachi S-3500N Scanning electron microscope (SEM), (Hitachi, Tokyo, Japan) was used to obtain energy dispersive X-ray (EDX) spectra, and Raman microscopy WiTec Access 300 equipment with a 532 nm laser. X-ray photoelectron spectroscopy (XPS) was determined by means of a VG-Microtech Multilab 3000. JEOL JEM 2100 equipment was used to obtain transmission electron microscopic (TEM) micrographs and a Bruker D-8 Advance diffractometer was used to record X-ray diffraction (XRD) peaks. Thermal characterization was performed with a DSC-822e type differential scanning calorimeter (DSC), between 0 and 140 °C, at a heating rate of 10 °C/min. TGA 1 HT type thermogravimetric analyzer (TGA) (Mettler-Toledo, USA) was used under a nitrogen atmosphere (50 ml/min) at a heating rate of 10 °C/min, under a nitrogen atmosphere (50 ml/min). Q800 (TA Instruments, USA) equipment was used for dynamic mechanical analysis (DMA), under the single cantilever configuration, in the temperature range between 30 and 145 °C, at a heating rate of 3 °C/min, with a frequency of 1 Hz, in ambient atmosphere.

Surface roughness and wear volumes were determined by means of a Talysurf CLI 500 (Taylor Hobson, U.K.) profilometer. Reciprocating sliding tribological tests with AISI 316L balls (1.6 mm diameter) against PMMA injected parts were carried out using a TRB tribometer (Anton Paar, Switzerland), under a normal applied load of 1 N, with a sliding frequency of 2 Hz, and a stroke length of 5 mm. Coefficients of friction were continuously recorded during each test. Tests were carried out on both the exterior and core surfaces under sliding directions parallel or perpendicular to the melt flow. Average friction coefficient and wear values were calculated after at least three tests.

Abrasion tests under multiple scratching were carried out according to ASTM D7027-05, using an MTR 3/50-50/NI microscratch (Microtest S.A., Spain) tester, with a diamond indenter (200 nm sphere radius) being used for multiple scratch (15 successive scratches) abrasive wear tests, under a normal applied load of 10 N, at a sliding velocity of 5 mm/min, with a sliding distance of 5 mm. Average instantaneous penetration (Pd), residual depth (Rd), and viscoelastic recovery values were calculated after at least three tests. All tribological tests were carried out in ambient conditions, temperature: 25 °C and relative humidity: 37%.

The rheology of PMMA and of the nanocomposites was studied with a parallel plate rotational rheometer (Ar-G2; TA Instruments, USA), at a temperature of 245 °C.

3. Results and discussion

3.1. Materials characterization

The results of XPS surface analysis of GOIL show the characteristic binding energies of F1s from the tetrafluoroborate anion and N1s from the imidazolium cation, while GO only presents C1s and O1s peaks, as previously described [29], although in the present case a lower IL proportion has been used to obtain the modified graphene oxide nanofiller GOIL (Figure 1).

X-ray diffraction patterns Figure 2 show the displacement of the maximum diffraction peak for GO to a lower angle (higher interlayer distance) when it is modified by IL.

GOIL diffraction pattern also shows the peaks at 22° and at 5°, which are also present in the IL.

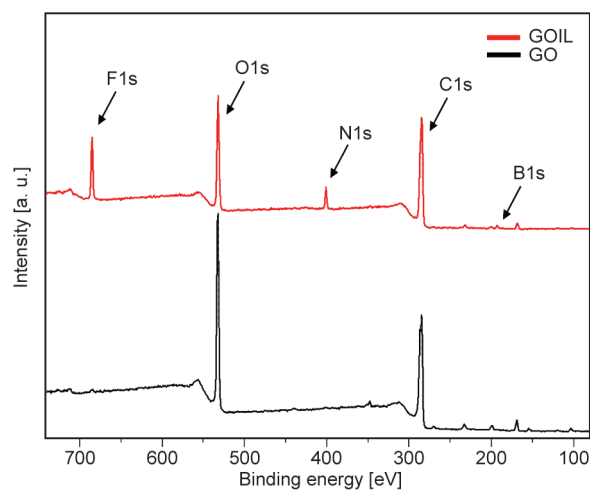


Figure 1. XPS surface analysis spectra for GO and GOIL.

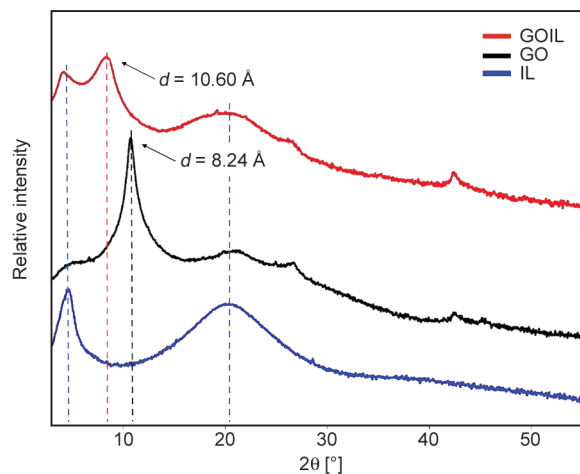


Figure 2. XRD diffractograms of GO; IL; and GOIL.

XPS and XRD results confirm the presence of the IL both at the outer surface and at the GO interlayer distance.

TEM micrographs of PMMA+GO and PMMA+GOIL (Figure 3) show the presence of GO or GOIL platelets inside the PMMA matrix. The presence of folded multilayers inside both nanocomposites could be a result of processing conditions.

The SEM micrograph (Figure 4) of the cryofracture surface of PMMA+GOIL shows the characteristic fragile fracture morphology. The presence of the IL phase was confirmed by the EDX spectrum of the selected area (Figure 4), which shows the presence of fluorine from the tetrafluoroborate anion.

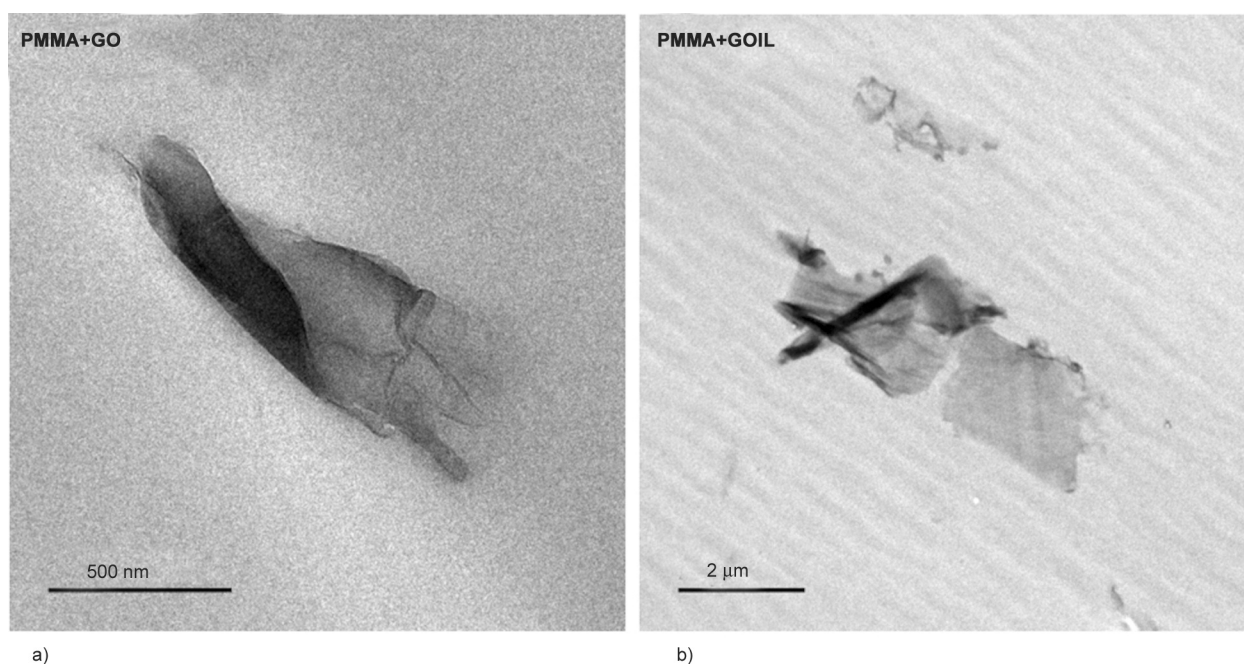


Figure 3. TEM micrographs of a) PMMA+GO and b) PMMA+GOIL.

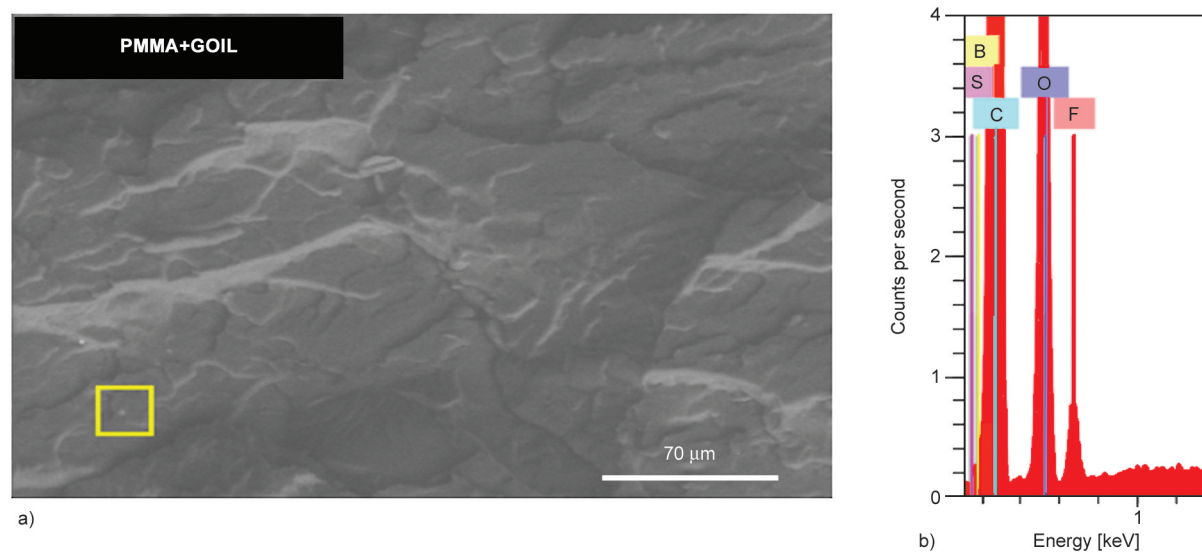


Figure 4. a) SEM micrograph of the cryofracture surface of PMMA+GOIL and b) EDX spectrum of the selected region.

Table 1 shows that glass transition temperatures (T_g), as determined by DSC, are similar for all materials, thus indicating no significant changes in chain mobility in the bulk materials induced by the nanofiller additives. The highest degradation temperature (T_d) (determined by TGA) is observed for PMMA+GOIL nanocomposite, as a result of the higher thermal stability of IL and GOIL with respect to PMMA [29].

Table 2 shows the values of the storage modulus onset (E'_{onset}), loss modulus maximum (E''_{peak}), and loss tangent ($\tan \delta$) maximum ($\tan \delta_{\text{peak}}$), and glass transition temperature values at the onset of storage modulus ($T_g (E'_{\text{onset}})$), at the maximum peak of loss modulus ($T_g (E''_{\text{peak}})$) and at the maximum peak of loss tangent ($T_g (\tan \delta_{\text{peak}})$). As observed in **Table 2**, DMA results are very similar for all materials. Glass transition temperatures and $\tan \delta$ values are the same for PMMA and both nanocomposites. Thus, GO and GOIL additives induce no significant changes in the viscoelastic behavior of injection molded PMMA, at least in the proportion added in the present work. This is also in agreement with the results previously obtained for similar nanocomposite extruded materials [29].

Figure 5 shows the D, G and 2D regions of the Raman spectra of the nanofillers and the nanocomposites.

Table 3 reports the position, intensity, the full width half maximum (FWHM) band width, and areas of each fitted peak.

A decrease in the intensity and FWHM of the D'' band has been related [31] to a crystallinity increase. According to this, as these values are higher for GOIL than for GO, (**Table 3**), the modification with ionic liquid produces a more amorphous hybrid nanofiller.

Table 1. Glass transition (T_g) and degradation (T_d) temperatures.

Material	T_g^* [°C]	T_d^{**} [°C]
PMMA	108.5±0.7	379.9±0.5
PMMA+GO	110.6±2.6	382.1±0.8
PMMA+GOIL	108.3±0.1	385.4±1.3

*Glass transition temperature

**Degradation temperature at 50% weight loss

Table 2. DMA results.

Material	E'_{onset} [MPa]	$T_g (E'_{\text{onset}})$ [°C]	E''_{peak} [MPa]	$T_g (E''_{\text{peak}})$ [°C]	$\tan \delta_{\text{peak}}$ [-]	$T_g (\tan \delta_{\text{peak}})$ [°C]
PMMA	3141.0±89.1	117.9±0.1	258.0±1.6	118.0±0.1	1.5±0.1	133.5±0.1
PMMA+GO	3066.0±45.2	118.7±0.6	260.2±0.1	119.1±0.6	1.5±0.1	134.1±0.6
PMMA+GOIL	3244.5±91.2	117.8±0.4	270.7±1.1	118.1±0.4	1.5±0.1	133.5 ±0.7

The position of the 2D band is shifted from 2711 cm^{-1} for GO, to 2705 cm^{-1} for GOIL. This decrease is in agreement with a lower content of sp^2 carbon [30]. In the same way, the slight increase in the I_D/I_G ratio (**Table 4**), from 0.92 for GO to 1.06 for GOIL shows a higher proportion of defects and the sp^3 bonds due to the presence of the IL [32, 33]. Crystallite size (L_A) [34] indicates a decrease in crystallinity or in sp^2 carbon [30, 35] and is also lower for GOIL than for GO (**Table 4**), in agreement with the reduction of sp^2 carbon.

The nanocomposites show the lowest crystallite size (**Table 4**) due to the degradation of the nanofillers after the extrusion and injection processing steps.

The effect of injection flow and nanophase orientation is also seen in surface roughness values. Surface topography and average roughness show a significant difference between the exterior and core section surfaces.

Table 5 and **Figure 6** show, respectively, average roughness values and surface topography profiles of PMMA and the nanocomposite materials, both on the exterior surface, which has been in contact with the mold wall [36, 37] and on the core section. The cutting operation to obtain core sections yields very similar R_a values for all materials (**Table 5**).

As expected, roughness values are higher on the exterior surface than on the core section, but this difference is much higher for the nanocomposites than for neat PMMA, which shows similar surface topography and roughness values on both surfaces. The addition of GO increases surface roughness of the exterior surface by a factor of 3.8. In the presence of the IL, in PMMA+GOIL, the roughness increases by a factor of 3.3 with respect to PMMA at the exterior surface. The very high exterior surface roughness of the nanocomposites could increase friction coefficients and wear rates.

3.2. Reciprocating sliding wear tests

In order to study the effect of the nanofiller additives, flow injection and surface topography on the tribological performance of PMMA, reciprocating sliding

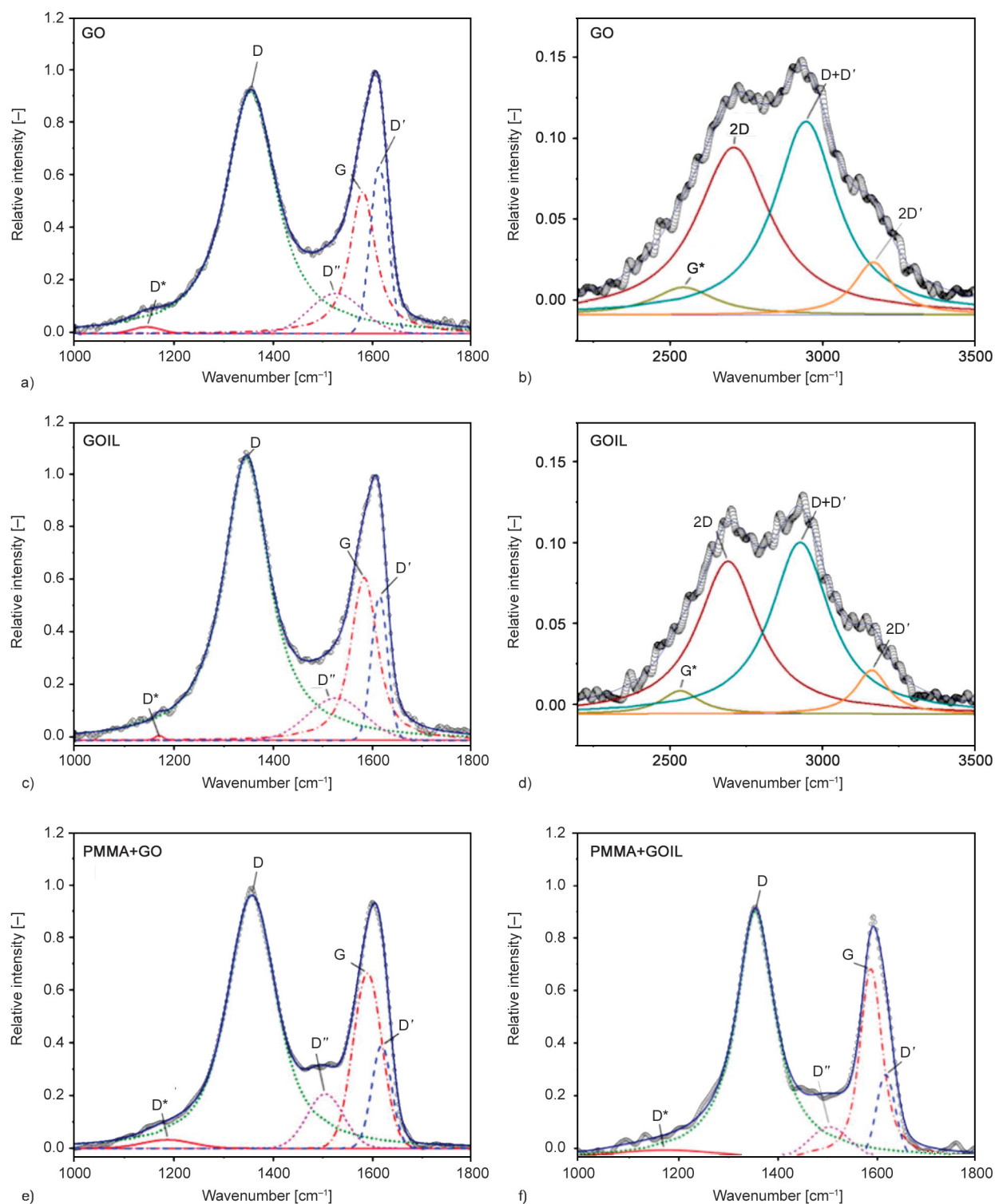


Figure 5. Raman spectra and deconvolution of D, G and 2D bands ($R^2 > 0.99$). a) GO bands D, G; b) GO band 2D; c) GOIL bands D, G; d) GOIL band 2D; e) PMMA+GO band D, G and f) PMMA+GOIL band 2G.

wear tests were performed on both the exterior and the longitudinal core section surfaces, as shown in [Figure 7](#).

[Figure 8](#) shows the characteristic coefficient of friction versus distance curve which are obtained for PMMA and nanocomposites under reciprocating sliding.

Initial or break-in friction coefficient (μ_0) values of approximately 0.10 and final or steady-state friction (μ_f) of 0.60 are obtained. All materials show transition distance values (d) lower than 100 m. Low initial friction coefficients are only maintained without transition to higher values during the whole sliding

Table 3. Raman results.

Nanophase	GO				
Band	D*	D	D''	G	D'
Wavenumber [cm ⁻¹]	1144.2	1354.6	1526.2	1580.1	1613.5
FWHM* [cm ⁻¹]	68.7	122.5	123.9	62.3	42.6
Area [%]	0.7	61.3	7.9	18.7	11.3
Relative intensity [-]	0.025	0.922	0.153	0.540	0.636

Nanophase	PMMA+GO				
Band	D*	D	D''	G	D'
Wavenumber [cm ⁻¹]	1187.0	1356.7	1504.4	1589.5	1618.0
FWHM* [cm ⁻¹]	120.5	118.7	86.5	68.5	47.0
Area [%]	1.7	62.3	7.9	20.1	8.1
Relative intensity [-]	0.032	0.962	0.207	0.664	0.390

*Full width at half maximum

Nanophase	GOIL				
Band	D*	D	D''	G	D'
Wavenumber [cm ⁻¹]	1169.1	1345.4	1526.7	1583.0	1613.9
FWHM* [cm ⁻¹]	20.1	111.2	134.6	63.7	38.3
Area [%]	0.1	62.9	8.6	20.1	8.3
Relative intensity [-]	0.017	1.077	0.161	0.619	0.549

Nanophase	PMMA+GOIL				
Band	D*	D	D''	G	D'
Wavenumber [cm ⁻¹]	1170.0	1355.6	1503.4	1588.0	1617.1
FWHM* [cm ⁻¹]	262.2	93.9	93.0	53.1	44.6
Area [%]	3.7	60.0	5.4	23.9	7.0
Relative intensity [-]	0.030	0.937	0.116	0.716	0.314

Table 4. Raman bands intensity ratios and sp² crystallite size (L_A) values.

Material	I_D/I	I_{2D}/I	L_A [nm]
GO	0.92±0.02	0.14±0.01	20.9
GOIL	1.06±0.04	0.14±0.01	18.1
PMMA+GO	1.08±0.04	–	17.8
PMMA+GOIL	1.10±0.08	–	17.5

Table 5. Surface roughness

Material	Roughness, R_a [μm]	
	Exterior	Core section
PMMA	0.18±0.01	0.15±0.01
PMMA+GO	0.69±0.05	0.17±0.01
PMMA+GOIL	0.60±0.04	0.15±0.01

test for the low roughness core section surface of PMMA+GO nanocomposite.

Figure 9 shows surface topography images of the wear tracks on all materials as a function of sliding direction, either parallel or perpendicular to the injection flow.

Wear volumes were determined from the product of cross-section worn areas [$A1-(A2+A3)$] [37] (where $A1$ is the area below the surface and $(A2+A3)$ are the areas of plastically deformed material accumulated on the edges of the wear track), along the length of the wear track (4 mm), without considering both wear track ends.

On the external surface, PMMA shows similar wear rates for both sliding directions, of the order of 10^{-3} mm³. In contrast, in PMMA+GO, the addition of GO reduces wear volume on the external surface in one order of magnitude, up to 10^{-4} mm³ (with

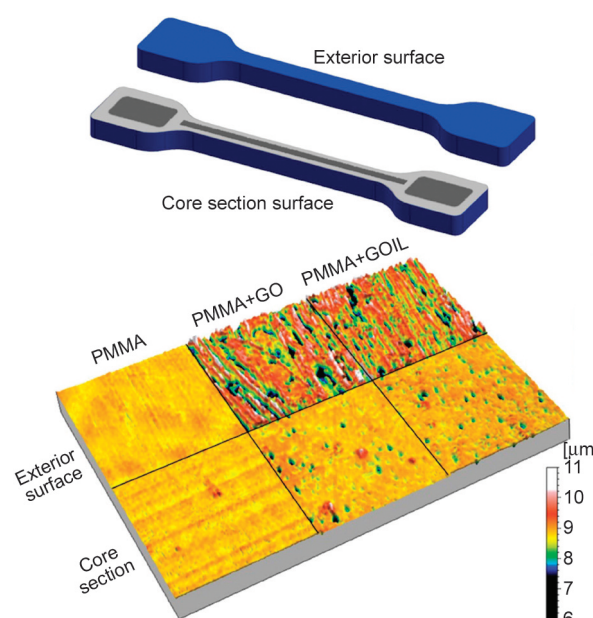


Figure 6. Scheme showing exterior and core section surfaces of injected parts and surface topography for PMMA, PMMA+GO and PMMA+GOIL on exterior and core section surfaces.

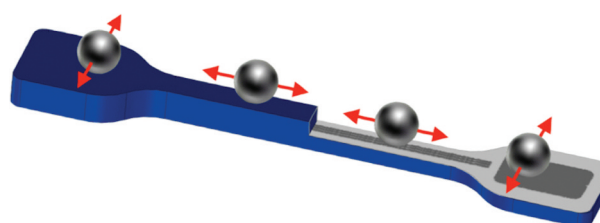


Figure 7. Scheme showing AISI 316L ball reciprocating sliding directions on PMMA and nanocomposites.

standard deviations lower than 10%). Moreover, PMMA+GO shows negligible wear volume on the core section surface, under both sliding directions, in agreement with the extremely mild surface damage shown in Figure 9. For PMMA+GOIL, surface damage is also minimized, but only under sliding

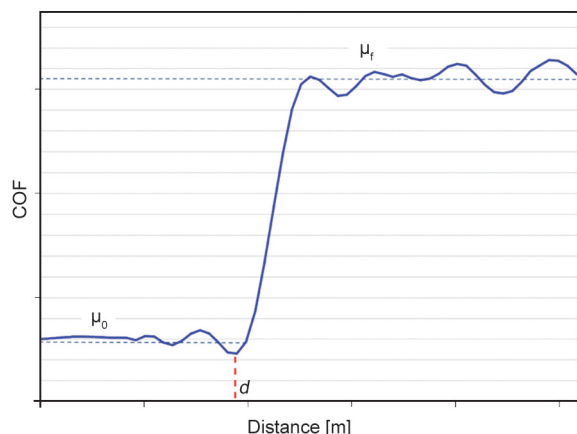


Figure 8. Representative coefficient of friction (COF) vs sliding distance record, under reciprocating sliding, showing transition distance from running-in (μ_0) and steady-state (μ_f).

parallel to the injection flow, in agreement with the longer transition distance of friction coefficients. Under sliding perpendicular to the flow, the wear volume of PMMA+GOIL is of the same order of magnitude as that of PMMA.

Wear scars on the different materials after reciprocating sliding tests were also studied by SEM microscopy.

Figure 10 shows SEM micrographs of the wear scars on core section surfaces. PMMA presents the same surface damage after sliding parallel and perpendicular to flow. Plastic deformation produces smooth

grooves with an accumulation of wear debris particle powder on the edges and at the ends of the scar.

Figure 10 shows very mild surface damage on PMMA+GO for both sliding directions. Wear debris is only observed in a very small amount compared to PMMA.

Figure 10 also shows the influence of sliding direction on PMMA+GOIL. Whilst in the parallel direction, the surface damage is very mild, similar to that observed for PMMA+GO. The wear damage in the perpendicular direction is more severe but shows a stick-slip effect, and some wear debris along the edges of the groove.

SEM micrographs in Figure 11 show the very mild abrasion wear parallel marks on PMMA+GO cross-section surface after reciprocating sliding in the direction parallel to flow.

A Raman study was carried out for a selected region inside the wear path (Figure 11). Raman mapping enables rich GO regions to be identified inside the PMMA matrix, as confirmed by their respective Raman spectra. GO-containing particles (in red), are randomly oriented inside the PMMA matrix (in blue). In order to study the distribution of the nanophases inside the colorless PMMA matrix, different cross-sections of the injected parts were obtained. Figure 12 (top) shows the results of an image composition of digital photographs along the longitudinal cross-sections of PMMA+GO, and PMMA+GOIL. Figure 12

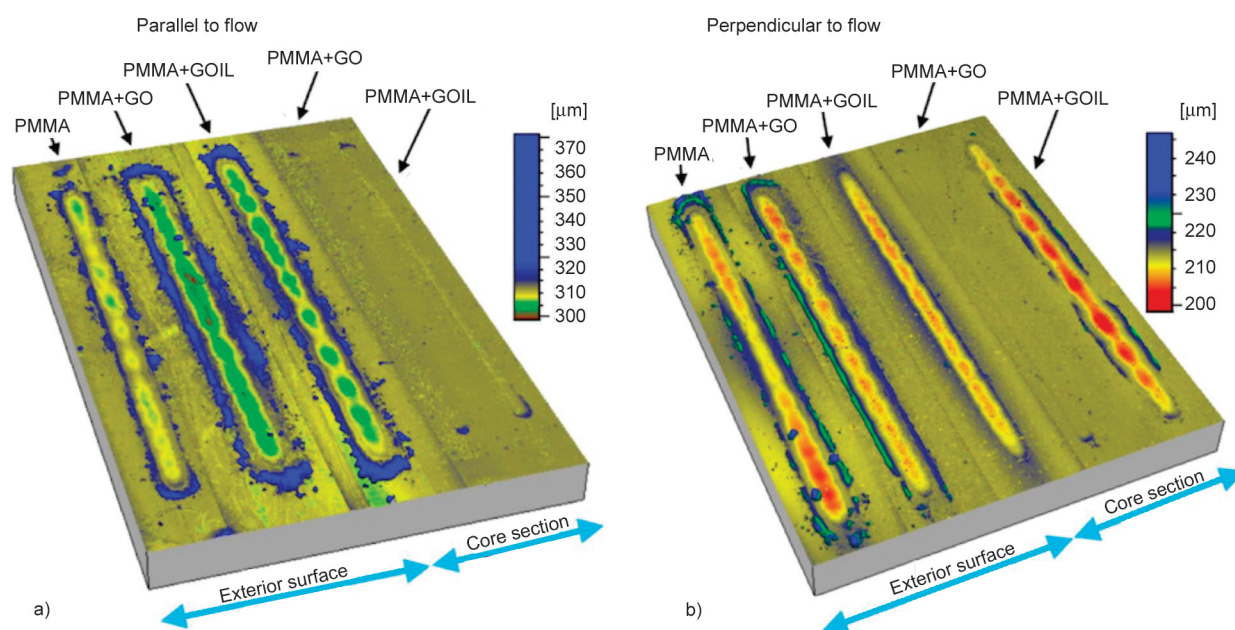


Figure 9. Profilometer surface topography of wear tracks after reciprocating sliding in the directions a) parallel to flow and b) perpendicular to flow.



Figure 10. SEM micrographs of wear tracks under sliding parallel and perpendicular to injection flow for PMMA, PMMA+GO and PMMA+GOIL.

also shows a front view of the apparent GO distribution inside PMMA+GO, and a composition of photographs of cross-sections perpendicular to the injection flow in the Gate region (closer to the mold feeding gate) and parallel to the injection flow in the End region.

Apparently, an expansion of the region occupied by the nanophase takes place inside the central channel. According to Dericiler *et al.* [38], the maximum velocity in injection flow samples of PA66 with graphene nanoplatelets is reached inside the narrower central channel. Results showed a variation in the orientation of graphene nanoplatelets along the length of the injected part.

As the weight percentage of the nanophases is the same along the injected part (as determined according to the ASTM D1603 standard), the optical observations in Figures 13 and 14 could be due to a different orientation and distribution of GO or GOIL along the injected parts geometry. Previous studies

on the orientation of carbon nanophases, in particular carbon nanotubes in molded polyvinylfluoride [39], have shown that the nanotubes are oriented parallel to the injection flow close to the mold wall but adopted a disordered orientation in the central core region. A Raman microscopy study was carried out in order to confirm the evolution of the orientation, at least of micron-size agglomerates, inside the injected parts section.

Figure 13 shows optical micrographs and Raman spectra of PMMA matrix and GO nanophase. Figure 14 shows the corresponding Raman study for PMMA+GOIL.

In both cases (Figures 13 and 14), it can be observed that the orientation of GO and GOIL additives is parallel to injection flow inside the regions closer to both exterior surfaces (top and bottom magnifications), and changes to a higher angle, including perpendicular orientation, with respect to the injection flow direction, inside the center region (central

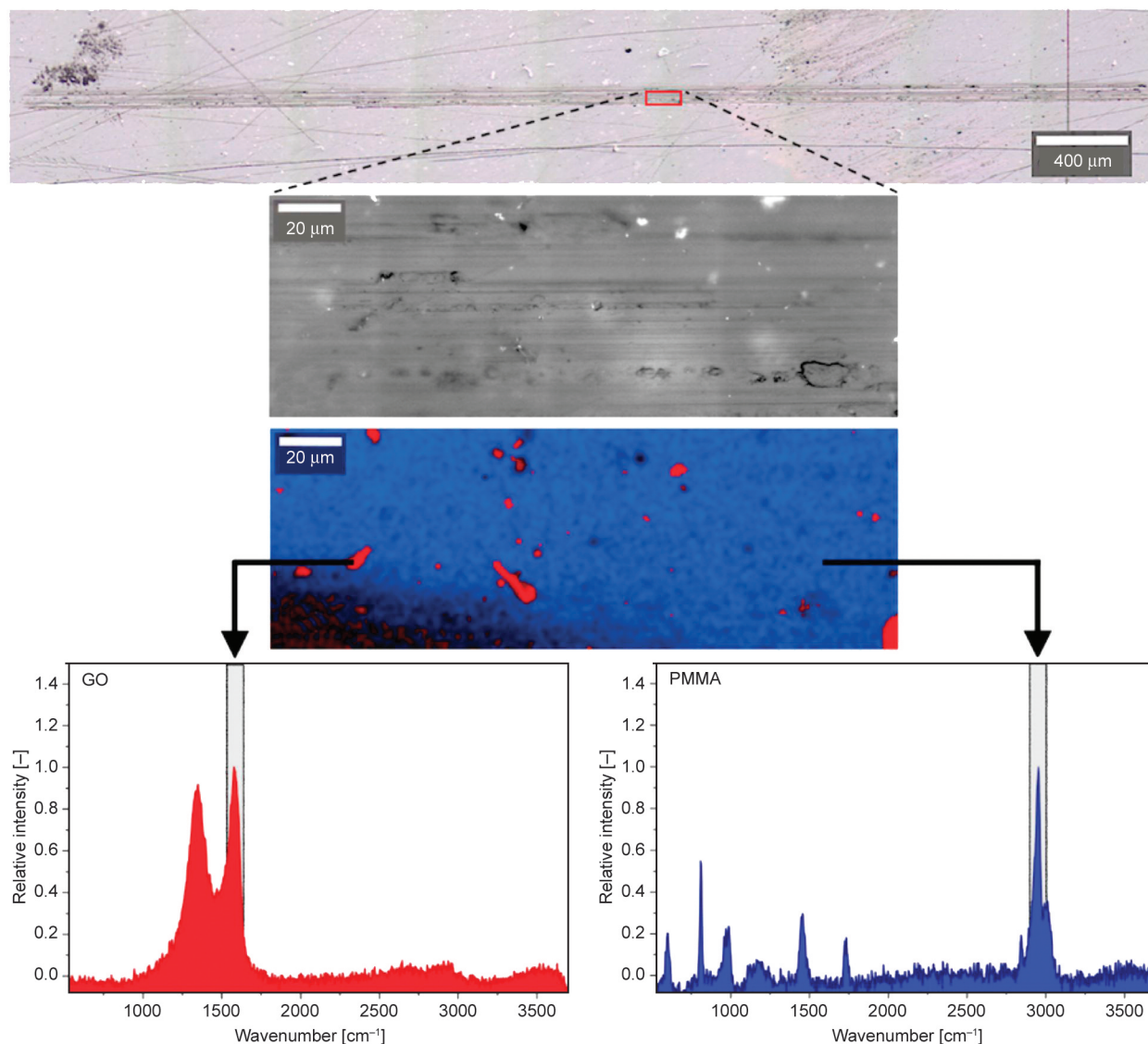


Figure 11. Raman micrograph of the wear scar after sliding parallel to the flow on PMMA+GO core section surface. Magnification of the selected area and Raman map and spectra of PMMA matrix (in blue) and GO nanofiller (in red). Highlighted in grey are the Raman bands used to obtain the Raman map.

magnification image) across the thickness of the injected part.

In all cases, the Raman spectra are in agreement with PMMA matrix (shown in blue) and GO or GOIL nanofillers (shown in red), respectively.

3.3. Abrasive wear tests under multiple scratching

Multiple scratch tests were performed in order to study the abrasion resistance of the new nanocomposites and their ability for viscoelastic recovery. The results of the oscillatory tests described in the previous section have shown the influence of sliding direction with respect to the injection flow, with higher resistance to surface damage under sliding in

the parallel direction. Previous results on the resistance of nanocomposites to abrasion under multiple scratching have also shown a similar effect [40].

With these precedents, the multiple scratch tests for the new nanocomposites were performed on the core section surfaces of the injected parts (see Figure 6), in the direction parallel to flow.

Figure 15 shows the Raman microscopy study of scratch grooves [41] on PMMA+GO. The magnification in Figure 15 shows the presence of very scarce surface defects and microcracks. Finally, GO particles (in red, in Figure 15) show a non-parallel alignment with respect to the injection flow or to the indenter pass at the core section level. These results show that the original orientation of the additives through the

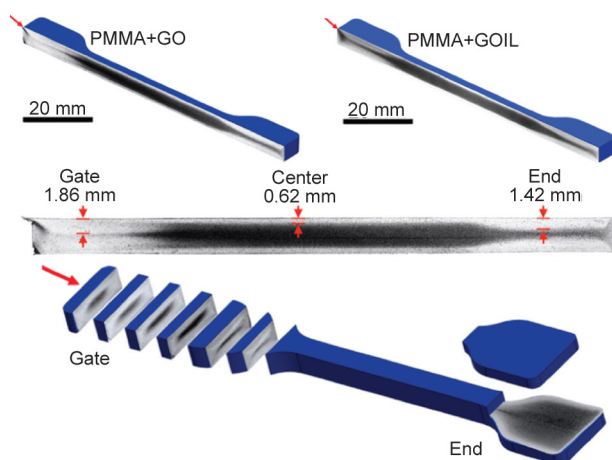


Figure 12. From top to bottom: longitudinal cross-section of PMMA+GO and PMMA+GOIL; front view of the longitudinal cross-section showing thickness of more transparent regions, and perpendicular cross-sections along the Gate region, and parallel core section along the End region. The arrows show the injection flow direction.

thickness of PMMA composites (Figure 13) is not altered under multiple scratching conditions.

Table 6 shows the results of instantaneous penetration (Pd), residual depth (Rd), and viscoelastic recovery

percentage (calculated as $[(Pd - Rd)/Pd] \cdot 100$) for each material. The best performance is found for the material containing graphene oxide modified by ionic liquid. Thus, although instantaneous penetration is higher for PMMA+GOIL than for PMMA+GO, PMMA+GOIL presents a higher viscoelastic recovery. This gives a final permanent damage (Rd) for PMMA+GOIL 21% lower than that for PMMA+GO. This behavior is attributed to the presence of the IL fluid phase and is in agreement with previous results [37]. The fluid ionic liquid phase increases polymer chain displacement and plastic deformation under load but also eases the viscoelastic recovery of the material.

The reinforcing effect of the addition of GO reduces plastic deformation and material loss under all sliding configurations and sliding directions studied here.

The results of multiscratch tests have shown that the mechanism in the case of the hybrid GOIL nanofiller is not the same. Although plastic deformation under load is higher than that of PMMA, the final surface damage is lower. This could be explained by an

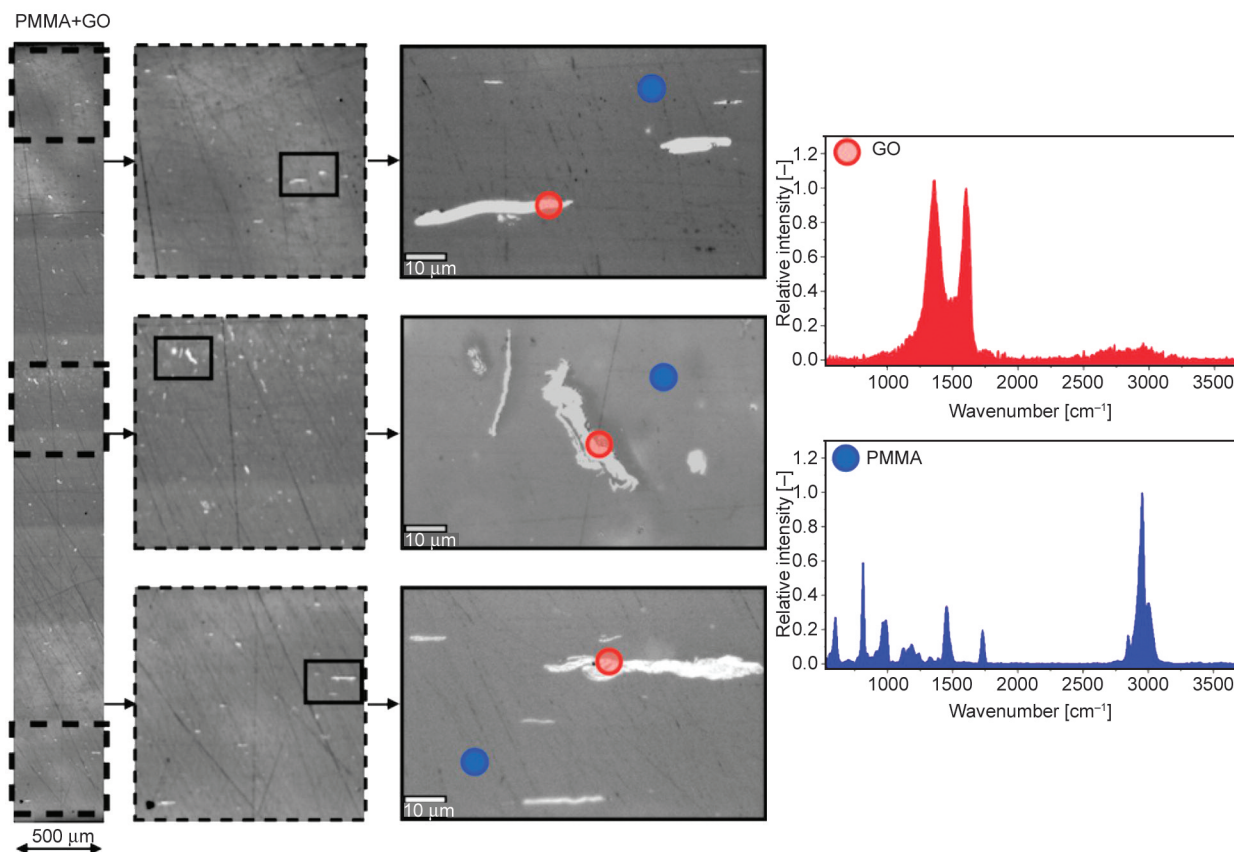


Figure 13. Optical microscopy (100×) images through the thickness of an injected part of PMMA+GO and Raman spectra of the matrix (in blue) and nanofiller (in red).

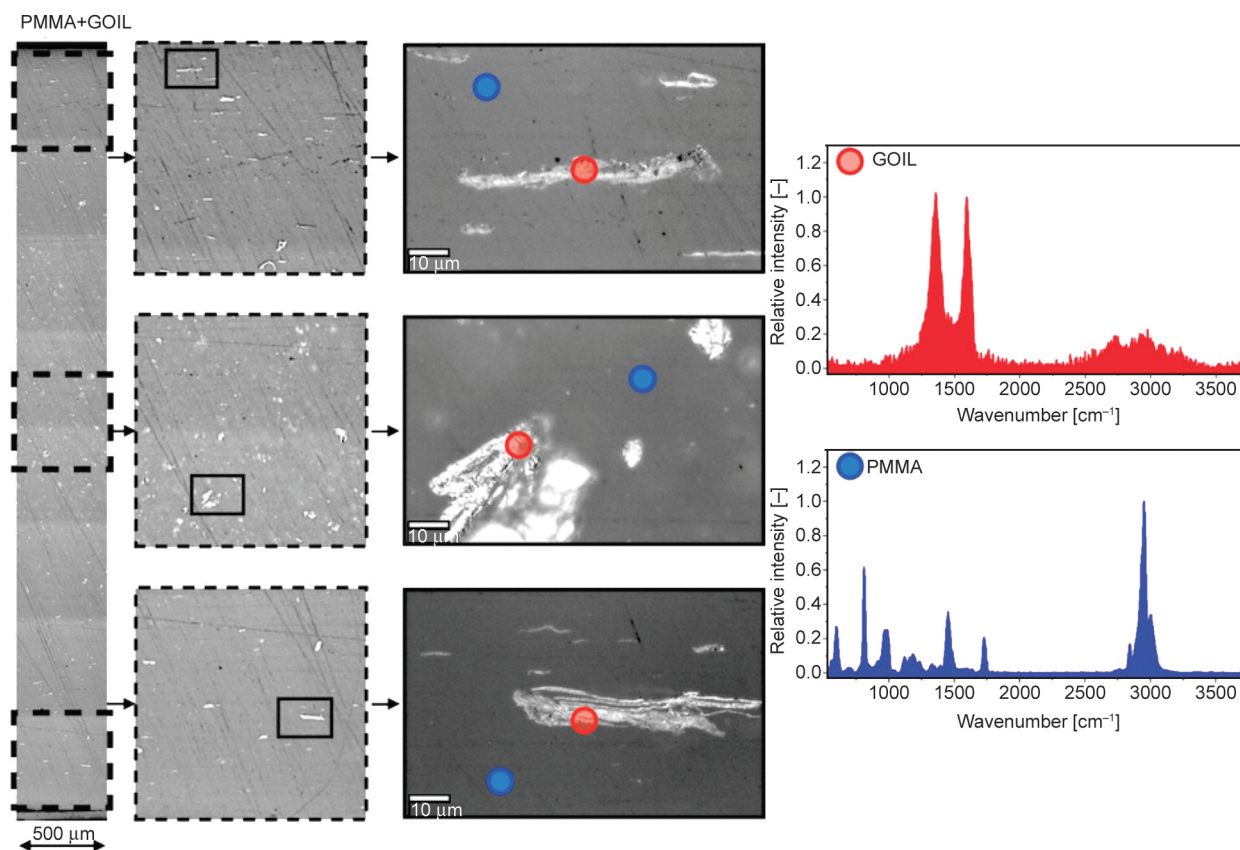


Figure 14. Optical microscopy (100×) images through the thickness of an injected part of PMMA+GOIL and Raman spectra of the matrix (in blue) and nanofiller (in red).

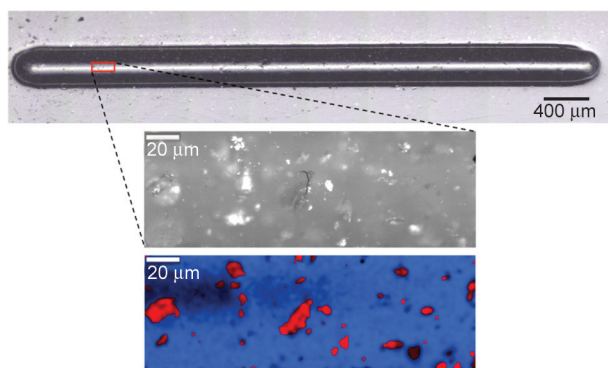


Figure 15. Optical microscopy image of wear scar on the core section surface of PMMA+GO after scratch test, magnification of the selected area and Raman map showing graphene oxide (red) in the PMMA matrix (blue).

Table 6. Abrasive wear resistance under multiple scratching on the core section surface (after 15 successive scratches on the same groove, parallel to flow).

Material	Pd [μm]	Rd [μm]	Recovery [%]
PMMA	68.6±2.7	24.5±0.9	64.3±2.4
PMMA+GO	49.8±2.5	19.2±1.3	61.5±2.6
PMMA+GOIL	75.5±5.5	15.2±1.2	79.7±2.4

internal effect of GOIL that induces localized mobility of PMMA chains under applied load. This mobility is mainly favored in the direction parallel to injection flow, as pointed out by the reciprocating sliding tests (section 3.2).

3.4. Rheological behavior

The rheological behavior of the materials in the softened state was studied in order to establish the influence of the additives on the resistance to flow of PMMA.

Complex viscosity values for PMMA+GO are very similar to those of PMMA (Figure 16), up to the highest angular frequency values, where PMMA+GO presents a sharp transition to higher viscosity values. PMMA+GOIL presents the lowest complex viscosity values (Figure 16) in the whole range of angular frequency. This confirms the ability of GOIL to improve the relative displacements of the polymer chains.

As complex viscosity is a measure of resistance to flow, the results shown in Figure 16, indicate that the ionic liquid phase could act as a processing aid, and

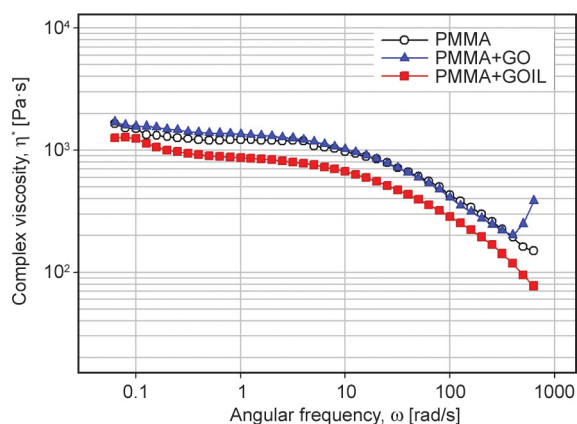


Figure 16. Variation of complex viscosity with angular frequency at 245 °C.

enhance viscoelastic recovery, as we have seen in multiple scratch tests.

4. Conclusions

Extrusion+injection molding melt processing has been used to obtain new PMMA nanocomposites with graphene oxide (GO) or graphene oxide modified by a room-temperature ionic liquid (GOIL), without the use of organic solvents.

Raman characterization of the new nanocomposites shows that modification with IL increases the defects and sp^3 bonds and reduces crystallinity in GO. The crystallite size of the nanophases is reduced when added to the PMMA matrix as a result of degradation induced by the extrusion+injection processing stages. Raman microscopy shows the heterogeneous orientation of the additives inside the polymer matrix, from predominantly parallel to the injection flow at both exterior surfaces, close to the injection mold walls, to a higher angle, including perpendicular orientation, inside the core section furthest from the mold walls.

The wear resistance of the new nanocomposites has been studied under reciprocating sliding both on the exterior and on the core section surfaces of the injected parts.

On the exterior surface, the tribological performance of PMMA+GO and PMMA+GOIL is similar to that of PMMA. This is attributed to the high surface roughness of the surface of the nanocomposite with respect to that of unmodified PMMA.

On the core section surface, with low surface roughness values, similar for all materials, PMMA+GO shows outstanding tribological performance with non-measurable wear under reciprocating sliding

both parallel and perpendicular to the injection flow due to the reinforcing effect of graphene oxide.

For PMMA+GOIL, negligible surface damage is only observed under sliding parallel to the flow, when the enhanced chain displacement ability of the IL fluid phase can be more effective.

In abrasion tests under multiple scratching on the core surface, in the direction parallel to flow, the nanocomposites reduce permanent surface damage of PMMA. In agreement with the reinforcing effect of GO, the highest resistance to instantaneous damage is reached for PMMA+GO, although the maximum viscoelastic recovery is observed for PMMA+GOIL. This is also attributed to the higher chain mobility induced by the presence of the fluid ionic liquid phase, which enhances instantaneous deformation under load but also viscoelastic recovery after the load is removed.

The ionic liquid modified graphene oxide additive could also act as a processing aid due to its ability to lower the complex viscosity of PMMA in the softened state.

The results presented herein highlight the different antiwear mechanism induced by each nanofiller and the relevance of processing parameters on the tribological behavior of the different regions of nanocomposite injected parts.

Acknowledgements

This research was funded by Spanish Ministerio de Ciencia e Innovación, Agencia Estatal de Investigación (AEI), and the European Union FEDER Program (Grants # MAT2017-85130-P and PID2021-122169NB-I00), and by the Fundación Seneca, Agencia de Ciencia y Tecnología de la Región de Murcia ('Ayuda a las Unidades y Grupos de Excelencia Científica de la Región de Murcia'; Grant # 19877/GERM/15).

References

- [1] Unal H., Mimaroglu A.: Friction and wear behaviour of unfilled engineering thermoplastics. *Materials and Design*, **24**, 183–187 (2003).
[https://doi.org/10.1016/S0261-3069\(03\)00018-9](https://doi.org/10.1016/S0261-3069(03)00018-9)
- [2] Brostow W., Lobland H. E. H., Hnatchuk N., Perez J. M.: Improvement of scratch and wear resistance of polymers by fillers including nanofillers. *Nanomaterials*, **7**, 66 (2017).
<https://doi.org/10.3390/nano7030066>
- [3] Sun J., Du S.: Application of graphene derivatives and their nanocomposites in tribology and lubrication: A review. *RSC Advances*, **9**, 40642–40661 (2019).
<https://doi.org/10.1039/C9RA05679C>

- [4] Chung D. D. L.: A review of multifunctional polymer-matrix structural composites. *Composites Part B: Engineering*, **160**, 644–660 (2019).
<https://doi.org/10.1016/j.compositesb.2018.12.117>
- [5] Friedrich K.: Polymer composites for tribological applications. *Advanced Industrial Engineering Polymer Research*, **1**, 3–39 (2018).
<https://doi.org/10.1016/j.aiepr.2018.05.001>
- [6] Trikkaliotis D. G., Christoforidis A. K., Mitropoulos A. C., Kyzas G. Z.: Graphene oxide synthesis, properties and characterization techniques: A comprehensive review. *ChemEngineering*, **5**, 64 (2021).
<https://doi.org/10.3390/chemengineering5030064>
- [7] Szeluga U., Kumanek B., Trzebicka B.: Synergy in hybrid polymer/nanocarbon composites. A review. *Composites Part A: Applied Science and Manufacturing*, **73**, 204–231 (2015).
<https://doi.org/10.1016/j.compositesa.2015.02.021>
- [8] Stankovich S., Dikin D. A., Dommett G. H. B., Kohlaas K. M., Zimney E. J., Stach E. A., Piner R. D., Nguyen S. T., Ruoff R. S.: Graphene-based composite materials. *Nature*, **442**, 282–286 (2006).
<https://doi.org/10.1038/nature04969>
- [9] Potts J. R., Dreyer D. R., Bielawski C. W., Ruoff R. S.: Graphene-based polymer nanocomposites. *Polymer*, **52**, 5–25 (2011).
<https://doi.org/10.1016/j.polymer.2010.11.042>
- [10] Kumar A., Sharma K., Dixit A. R.: A review of the mechanical and thermal properties of graphene and its hybrid polymer nanocomposites for structural applications. *Journal of Materials Science*, **54**, 5992–6026 (2019).
<https://doi.org/10.1007/s10853-018-03244-3>
- [11] Vallés C., Kinloch I. A., Young R. J., Wilson N. R., Rourke J. P.: Graphene oxide and base-washed graphene oxide as reinforcements in PMMA nanocomposites. *Composite Science and Technology*, **88**, 158–164 (2013).
<https://doi.org/10.1016/j.compscitech.2013.08.030>
- [12] Kausar A.: Poly(methyl methacrylate) nanocomposite reinforced with graphene, graphene oxide, and graphite: A review. *Polymer-Plastics Technology and Materials*, **58**, 821–842 (2019).
<https://doi.org/10.1080/25740881.2018.1563112>
- [13] Mirabedini A., Ang M., Nikzad M., Fox B., Lau K-T., Hameed N.: Evolving strategies for producing multi-scale graphene-enhanced fiber-reinforced polymer composites for smart structural applications. *Advanced Science*, **7**, 1903501 (2020).
<https://doi.org/10.1002/advs.201903501>
- [14] Song J., Zhang J., Lin C.: Influence of graphene oxide on the tribological and electrical properties of PMMA composites. *Journal of Nanomaterials*, **2013**, 846102 (2013).
<https://doi.org/10.1155/2013/846102>
- [15] Livi S., Duchet-Rumeau J., Gérard J-F., Pham T. N.: Polymers and ionic liquids: A successful wedding. *Macromolecular Chemistry and Physics*, **216**, 359–368 (2015).
<https://doi.org/10.1002/macp.201400425>
- [16] Scott M. P., Brazel C. S., Benton M. G., Mays J. W., Holbrey D., Rogers R. D.: Application of ionic liquids as plasticizers for poly(methyl methacrylate). *Chemical Communications*, **13**, 1370–1371 (2002).
<https://doi.org/10.1039/B204316P>
- [17] Scott M. P., Rahman M., Brazel C. S.: Application of ionic liquids as low-volatility plasticizers for PMMA. *European Polymer Journal*, **39**, 1947–1953 (2003).
[https://doi.org/10.1016/S0014-3057\(03\)00129-0](https://doi.org/10.1016/S0014-3057(03)00129-0)
- [18] Zhao L., Li Y., Cao X., You J., Dong W.: Multifunctional role of an ionic liquid in melt-blended poly(methyl methacrylate)/ multi-walled carbon nanotube nanocomposites. *Nanotechnology*, **23**, 255702 (2012).
<https://doi.org/10.1088/0957-4484/23/25/255702>
- [19] Zornio C. F., Livi S., Rumeau J. D., Gerard J-F.: Ionic liquid-nanostructured poly(methyl methacrylate). *Nanomaterials*, **9**, 1376 (2019).
<https://doi.org/10.3390/nano9101376>
- [20] Avilés M-D., Pamies R., Sanes J., Bermúdez M-D.: Graphene-ionic liquid thin film nanolubricant. *Nanomaterials*, **10**, 535 (2020).
<https://doi.org/10.3390/nano10030535>
- [21] Khare V., Pham M-Q, Kumari N., Yoon H-S., Kim C-S., Park J-L., Ahn S-H.: Graphene-ionic liquid based hybrid nanomaterials as novel lubricant for low friction and wear. *ACS Applied Materials and Interfaces*, **5**, 4063–4075 (2013).
<https://doi.org/10.1021/am302761c>
- [22] Avilés M-D., Saurín N., Sanes J., Carrión F-J., Bermúdez M-D.: Ionanocarbon lubricants. The combination of ionic liquids and carbon nanophases in tribology. *Lubricants*, **5**, 14 (2017).
<https://doi.org/10.3390/lubricants5020014>
- [23] Tunckol M., Durand J., Serp P.: Carbon nanomaterial-ionic liquid hybrids. *Carbon*, **50**, 4303–4334 (2012).
<https://doi.org/10.1016/j.carbon.2012.05.017>
- [24] Aldroubi S., Brun N., Malham I. B., Mehdi A.: When graphene meets ionic liquids: A good match for the design of functional materials. *Nanoscale*, **13**, 2750–2779 (2021).
<https://doi.org/10.1039/D0NR06871C>
- [25] Zhao F., Zhang L., Li G., Guo Y., Qi H., Zhang G.: Significantly enhancing tribological performance of epoxy by filling with ionic liquid functionalized graphene oxide. *Carbon*, **136**, 309–319 (2018).
<https://doi.org/10.1016/j.carbon.2018.05.002>
- [26] Sanes J., Avilés M. D., Saurín N., Espinosa T., Carrión F-J., Bermúdez M-D.: Synergy between graphene and ionic liquid lubricant additives. *Tribology International*, **116**, 371–382 (2017).
<https://doi.org/10.1016/j.triboint.2017.07.030>

- [27] Espejo C., Carrión F. J., Bermúdez M. D.: Scratch resistance of new polystyrene nanocomposites with ionic liquid-modified multi-walled carbon nanotubes. *Tribology Letters*, **52**, 271–285 (2013).
<https://doi.org/10.1007/s11249-013-0212-0>
- [28] Bermúdez M. D., Carrión F. J., Espejo C., Martínez-López E., Sanes J.: Abrasive wear under multiscratching of polystyrene + single-walled carbon nanotube nanocomposites. Effect of sliding direction and modification by ionic liquid. *Applied Surface Science*, **257**, 9073–9081 (2011).
<https://doi.org/10.1016/j.apsusc.2011.05.103>
- [29] Sanes J., Ojados G., Pamies R., Bermúdez M. D.: PMMA nanocomposites with graphene oxide hybrid nanofillers. *Express Polymer Letters*, **13**, 910–922 (2019).
<https://doi.org/10.3144/expresspolymlett.2019.79>
- [30] López-Díaz D., Holgado M. L., García-Fierro J. L., Velázquez M. : Evolution of the Raman spectrum with the chemical composition of graphene oxide. *The Journal of Physical Chemistry C*, **121**, 20489–20497 (2017).
<https://doi.org/10.1021/acs.jpcc.7b06236>
- [31] Claramunt S., Varea A., López-Díaz D., Velázquez M. M., Cirera A.: The importance of interbands on the interpretation of the Raman spectrum of graphene oxide. *The Journal of Physical Chemistry C*, **119**, 10123–10129 (2015).
<https://doi.org/10.1021/acs.jpcc.5b01590>
- [32] Lee A. Y., Yang K., Anh N. D., Park C., Lee S. M., Lee T. G., Jeong M. S.: Raman study of D* band in graphene oxide and its correlation with reduction. *Applied Surface Science*, **536**, 147990 (2021).
<https://doi.org/10.1016/j.apsusc.2020.147990>
- [33] Thomas K. J., Sheeba M., Nampoori V. P. N., Vallabhan C. P. G., Radhakrishnan P.: Raman spectra of polymethyl methacrylate optical fibres excited by a 532 nm diode pumped solid state laser. *Journal of Optics A: Pure and Applied Optics*, **10**, 055303 (2008).
<https://doi.org/10.1088/1464-4258/10/5/055303>
- [34] Cançado L. G., Takai K., Enoki T., Endo M., Kim Y. A., Mizusaki H.: General equation for the determination of the crystallite size L_a of nanographite by Raman spectroscopy. *Applied Physics Letters*, **88**, 163106 (2006).
<https://doi.org/10.1063/1.2196057>
- [35] Krishnamoorthy K., Veerapandian M., Yun Q., Kim S.-J.: The chemical and structural analysis of graphene oxide with different degrees of oxidation. *Carbon*, **53**, 38–49 (2013).
<https://doi.org/10.1016/j.carbon.2012.10.013>
- [36] Martínez-Mateo I., Carrión-Vilches F. J., Sanes J., Bermúdez M. D.: Surface damage of mold steel and its influence on surface roughness of injection molded plastic parts. *Wear*, **271**, 2512–2516 (2011).
<https://doi.org/10.1016/j.wear.2010.11.054>
- [37] Carrión-Vilches F. J., González-Vivas A., Martínez-Mateo I. J., Bermúdez M. D.: Study of the abrasion resistance under scratching of polybutylenetereftalateglass fiber composites. *Tribology International*, **192**, 365–378 (2015).
<https://doi.org/10.1016/j.triboint.2015.07.004>
- [38] Dericiler K., Sadeghi H. M., Yagci Y. E., Sas H. S., Okan B. S.: Experimental and numerical investigation of flow and alignment behavior of waste tire-derived graphene nanoplatelets in PA66 matrix during melt-mixing and injection. *Polymers*, **13**, 949 (2021).
<https://doi.org/10.3390/polym13060949>
- [39] Fan B., Lu X., Dang Z., Deng Y., Zhou X., He D., Bai J.: Improved dispersion of carbon nanotubes in poly(vinylidene fluoride) composites by hybrids with core-shell structure. *Journal of Applied Polymer Science*, **135**, 45693 (2018).
<https://doi.org/10.1002/app.45693>
- [40] Bermúdez M. D., Carrión F. J., Espejo C., Martínez-López E., Sanes J.: Abrasive wear under multiscratching of polystyrene + single-walled carbon nanotube nanocomposites. Effect of sliding direction and modification by ionic liquid. *Applied Surface Science*, **257**, 9073–9081 (2011).
<https://doi.org/10.1016/j.apsusc.2011.05.103>
- [41] Brostow W., Chonkaew W., Rapoport L., Soifer Y., Verdyan A., Soifer Y.: Grooves in scratch testing. *Materials Research Society*, **22**, 2483–2487 (2007).
<https://doi.org/10.1557/JMR.2007.0307>